Stability of Small MgO Nanotube Clusters: Predictions of a Transferable Ionic Potential Model

Mark Wilson

Physical and Theoretical Chemistry Laboratory, Oxford University, South Parks Road, Oxford OX1 3QZ, U.K.

Received: February 26, 1997[⊗]

The recently introduced compressible-ion interaction model (CIM) is extended to allow for coordination number-dependent oxide polarizabilities. The variable polarizability is parametrized from existing Hartree−Fock calculations. The resulting potential is used to examine small $(MgO)_n$ clusters in both their relaxed and unrelaxed (more symmetrical) structures. The results are compared to experimental results and both Hartree−Fock and density functional theory calculations. Comparison with alkali halide clusters is also made. The potential is found to be transferable over a wide range of ionic environments, spanning gas-phase clusters and the bulk phase. MgO nanotubes are found to be stable for small clusters of less than 30 molecules.

I. Introduction and Outline

The study of isolated clusters represents a strong challenge for a simple potential model, as it must be able to represent both the fully coordinated (bulk) sites and the undercoordinated (often surface) sites dominant in the small clusters.

The cluster chemistry of $(MgO)_n$ (n = cluster size) is of interest for a variety of reasons. Experimental mass spectroscopy measurements[1] show distinct peaks in the higher cluster mass range ($n > 30$), consistent with the formation of bulklike (B1, rocksalt structure) fragments. The smaller mass spectrum shows clear peaks at $n = 6$, 9, 12, 15, 18, 24, 27, and 30, that is, separated by $(MgO)_3$ units. Conflicting analyses in terms of $(MgO)_3$ units[2,3] and cube-based geometries[1] have been advanced to explain the same experimental data. More abstractly, $(MgO)_n$ clusters have been invoked to explain the formation of stellar bodies[4] in oxygen rich stellar environments. Furthermore, an understanding of the cluster growth could lead to the understanding of the epitaxial growth of the ideal surface.

The most extensive *ab initio* study on cluster properties has been performed by Ahlrichs *et al*., who focused on three alkali halides LiF, NaCl, and KCl.[5,6] These calculations show that the ground state geometries preferred by the low-mass LiF clusters differ from those favored by both NaCl and KCl. The latter two form clusters that have geometries dominated by bulk fragments. LiF, on the other hand, favors clusters based on stacking $(LiF)_3$ hexagons (nanotubes) in the low ($n < 27$) mass range. All three systems prefer bulklike geometries for $n > 30$.

Recio *et al*.[7] have performed an extensive set of Hartree−Fock calculations (and a less extensive set of the more expensive MP2 calculations) on MgO itself. The clusters are divided into ring-based and cube-based units with only specific (highly symmetric) geometries considered owing to the complexity of the calculations. Veliah *et al*.[8] have performed a limited set of DFT-based calculations on small clusters (although the technique allows for larger clusters than the HF calculations, up to 64 atoms). Although these results are somewhat "underanalyzed", the types of surface distortion characteristic of significant anion polarization effects are in evidence.[9]

Ziemann and Castleman[1] utilize rigid-ion models (RIMs) (pair-potentials without polarization effect) to analyze the mass spectra. Two models are used based on ionic charges of ±1 and ±2, respectively, the former being used in an attempt to model "covalent" effects. The larger (formal) charge RIM is found to favor more open cluster structures. Shell models (in which the dipole polarization effects are included within a particular traditional mechanical description) are found to have little effect on the results, although it is important to note that the authors highlight the difficulties in parametrizing the shell model[10] on the ion-pair data, forcing the use of a model parametrized on bulk data. The lower charge potential model favors more closely packed structures.

These calculations highlight a central problem addressed in this paper. A major difference between ions in the perfect bulk crystalline environment and those in (particularly) surface sites lies in the nonvanishing electric fields in the latter. The high asymmetry of the typical ion surface environment leads to the significant distortion of the ion electron density away from the spherical distribution typical of the bulk (polarization effects). The result is that, although the bulk properties of perfect crystals are generally describable via simple ionic models *excluding* polarization effects, this is not true for surfaces, defects, and, in particular, clusters in which the majority of ions find themselves in such asymmetric environments. For MgO we can confine ourselves to including anion polarization effects only, as the *ab initio* Mg^{2+} polarizability[11] is some 3 orders of magnitude smaller than that of the O^{2-} ion in the crystal.[12]

The general problems associated with simulating oxides are well-known. The O^{2-} ion is unstable in the free state, dissociating into O^- plus an electron, an effective infinite polarizability. The addition of the second electron is stabilized in the condensed environment by the crystal field (Madelung potential). The result is that the nature of the oxide anion is more dependent on the precise nature of the condensed environment than, say, a halide ion which is stable as a free species.[13] As a result a single effective pair-potential (EPP), parametrized from a single coordination number, does not transfer to other coordination numbers.[10,14,15] This problem is highlighted by the Watson-sphere-based calculations of Tossell,[16] which show how different Watson sphere charges are required to model the solid and molecule (the isolated ion pair), respectively. This requirement has severe implications for the transferability of such models. Transferable potentials can be generated by splitting the total short-range anion−cation energy into a rearrangement term, the energy required to take the ion in the free state and compress it into the crystalline environment,

[⊗] Abstract published in *Advance ACS Abstracts,* May 15, 1997.

S1089-5647(97)00712-8 CCC: $14.00

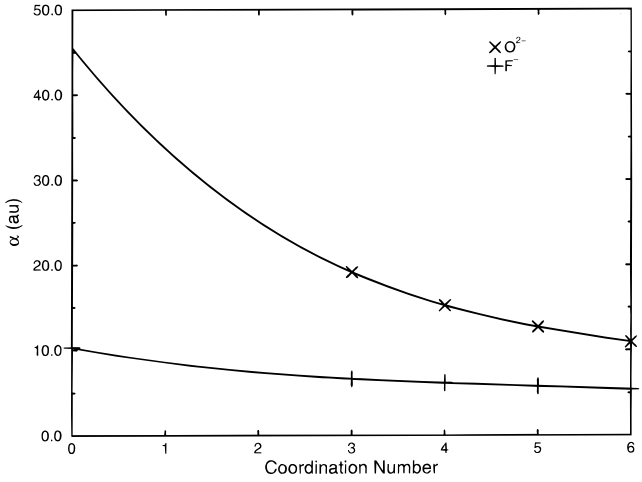

Figure 1. Oxide (×) and fluoride (+) dipole polarizability, α, against coordination number[17] with the polynomial fits (eq 2.1).

and an overlap term, giving the (repulsive) energy of interaction of the anion and the neighboring cations. The recently introduced compressible-ion model (CIM) allows for this spherical relaxation (breathing) of the anion by partitioning the anion−cation short-range energy into the overlap (with nearest-neighbor cations) and rearrangement terms. This model has been shown to give a much better representation of coordination number-dependent properties in MgO and CaO[14] and in ZrO_2[15] than can a single EPP. The inclusion of the anion "breathing" and the polarization effects introduce a many-body aspect into the potential model.

In the current work the true transferability of the CIM is tested to the limit. A single EPP cannot reproduce *both* the crystal lattice parameter *and* molecular bond length for MgO, unlike the halides.[1,16] This difference between the oxides and halides can again be attributed to the greater dependence of the nature of the oxide ion on its environment. In terms of the ionic model the ion pair and the crystal represent the two extrema. The ions in the crystal are in the most symmetric environment, while the ions in the ion pair are in the most unsymmetric possible environment.

A central problem associated with the *ab initio* study of such clusters lies in the large number of potential geometries that must be considered. The use of full *ab initio* methods to look at all possible geometries is not practicable because of the computational expense. Such calculations have often been simplified by minimizing the energy with respect to *specific* geometries guided by human imagination. The result is that the investigations have been confined to the more symmetric cluster geometries. We shall show that less symmetric geometries often appear energetically favorable. An aim here, therefore, is to use *ab initio* data as an input to a potential model and study a series of general cluster geometries with the potential model. The final geometries obtained from this study could then be used as starting points for additional *ab initio* calculations.

Fowler and Tole[17] have performed a series of Hartree−Fock *ab initio* calculations focusing on the O^{2-} anion in MgO both in the perfect rock salt crystal (six-coordinate anion) and on a surface face (five coordinate), on an edge (four coordinate), and on a corner (three coordinate). These calculations clearly demonstrate the environmental dependence of the dipole polarizability: it *decreases* as the coordination number *increases*. This is consistent with the known dependence of the affinity of the oxide anion to the second electron discussed above. Figure 1 shows the trace of the dipole polarizability tensor against the coordination number of the anion. The oxide polarizability clearly increases significantly as the coordination number is reduced. Also shown for comparison is the trace of the dipole polarizability for a fluoride anion in LiF calculated in the same manner.[17] The rise in polarizability with reduction in coordination number is much less dramatic in the fluoride case than in the oxide.

The rigid-ion calculation[1] using different ion charges coupled with the Watson-sphere-based calculations[16] suggests the possible role of charge-transfer effects in this system.[18] In terms of producing a relatively simple potential model a choice must be made between reducing the formal charges, on one hand, and including polarization effects while retaining formal charges (the two possibilities are essentially noncomplementary). Both effects can lead to properties typically ascribed to "covalency".[10] It is our belief, however, that the use of formal charges in conjunction with a proper description of the polarization effects is the best hope for producing truly *transferable* potential models since the *a priori* assignment of the full charge implies closed shell interactions.

In the current work both the compressible-ion and variable polarizability effects are included in a potential model, which is then compared both to *ab initio* calculations and experimental observation for both the ion pair and the crystal. Previous work allows us to predict the possible effects of including both the compressible ions and the anion dipole polarization effects. The CIM will tend to destabilize the undercoordinated anions sites (with respect to using an EPP), while the polarization effects will tend to make the oxide sites less symmetric.

II. The Model

A. Short-Range Terms. The basic CIM[14] derived on the basis described in the Introduction is used to model the anion−cation short-range interactions. This aspect of the potential model remains unchanged throughout all simulations: the ion pair and the crystals are simulated using the same short-range anion−cation interaction potential.

A model using the simple effective pair potential (EPP)[14] is also used for comparison. This model is derived from the *same ab initio* data as for the CIM and so gives equivalent results (to within the quality of the potential model fits) for the six-coordinate B1 phase. Differences will arise away from this coordination number.

B. Polarization Terms. In the previous CIM calculation on MgO[14] only the perfect four-coordinate, six-coordinate, and eight-coordinate crystal structures were considered. In this coordination number range the polarizability can reasonably be taken as constant, bearing in mind that in the static crystal calculations of the type performed the oxide polarizability affects only the dispersion terms which give a relatively small (although significant) contribution to the overall crystal energy.[11] In the current calculations the oxide anion environment is unlike the ideal crystals in both the low coordination numbers (in the range 1−6) and in the asymmetry of the environment, particularly on the surface layer itself. As a result, the basic polarizable-ion model[19] is augmented with a more appropriate coordination number-dependent oxide anion polarizability.

The coordination number (n) dependent polarizability is derived from Hartree−Fock *ab initio* calculations.[17] A fourth-order polynomial

$$\alpha(n) = an^3 + bn^2 + cn + d \qquad (2.1)$$

is fitted to the available three- to six-coordinate data in order to derive values corresponding to one and two coordination.

TABLE 1: Oxide and Fluoride Dipole Polarizability with Coordination Number[a]

coordination number	$\alpha_{O^{2-}}$	α_{F^-}
0 (free ion)	"∞"	10.321
1	33.651	8.575
2	25.081	7.404
3	19.158	6.654
4	15.251	6.170
5	12.728	5.800
6	10.957	5.388

[a] The coordinations 3−6 are from ref 17, the free ion fluoride value is from ref 13, and the 1 and 2 coordinate values are fitted.

TABLE 2: $an^3 + bn^2 + cn + d$ Polynomial Parameters for the Oxide and Fluoride Anions

coefficient	O^{2-}	F^-
a	−0.105 317	−0.025 667
b	1.955 779	0.364 40
c	−13.700 70	−2.084 55
d	45.501 64	10.320 81

The fit to the oxide *ab initio* data is shown in Figure 1 along with an analogous fit to the fluoride data, shown to further emphasize the greater coordination number dependence of the oxide polarizability. Although singly coordinate values are available for the oxide ion, these are very dependent upon the details of the *ab initio* calculation.[20] The derived polarizabilities are given in Table 1, with the polynomial coefficients in Table 2. Note that the fluoride curve goes through the "zero-coordinate" (free ion) value correctly. The "free" oxide finite value is simply an artifact of the model but has no bearing on the model, as this coordination number does not arise.

The effect of nearest-neighbor overlap on the anion dipoles must be considered.[10] In the PIM this is handled via a single-parameter (the short-range damping parameter (SRDP)) function.[19] Following previous work (for example ref 21), we choose to scale the SRDP for the ion pair by the anion−cation separation. This gives a value of around 1.80 for the molecule compared with 1.5 for the bulk. The larger value for the molecule reflects the smaller Mg−O separation and hence the shorter range of the overlap interaction.

C. Dispersion Terms. The variable nature of the oxide ion polarizability causes the dispersion terms to vary. In general the dispersion energy is given by

$$U^{\mathrm{disp}}(r^{ij}) = \sum_{n=6,8...}^{\infty} \sum_{i=2}^{N_t} \sum_{j=1}^{i-1} \frac{C_n^{ij}}{r^{ij^n}} f_n(r^{ij}) \qquad (2.2)$$

where C_n^{ij} is the dispersion coefficient relevant to the interaction between species *i* and *j* and f_n is a damping function representing the effect of the overlap of the electron densities of ions *i* and *j* (which acts to reduce a given dispersion energy term from its asymptotic value). Following the usual procedure,[22] the series is cut off at $n = 8$.

The dipole−dipole and dipole−quadrupole dispersion coefficients (C_6^{ij} and C_8^{ij}) are related to the dipole polarizabilities of species *i* and *j* via the Slater−Kirkwood formula[23] and Starkschall−Gordon formula,[24] respectively. The resulting coefficients are given in Table 3.

The dispersion damping coefficients are taken as those derived previously for MgO.[14] Previous work has demonstrated that these terms are necessary in order to reproduce experimental properties.[14] The exact expression derived by Jacobi and Csanak[25] (see also Pyper[11]) does not readily translate into a tractable molecular dynamics scheme. In keeping with previous work,[14] therefore, these functions are fitted externally to Tang−Toennies-like dispersion damping functions.[26]

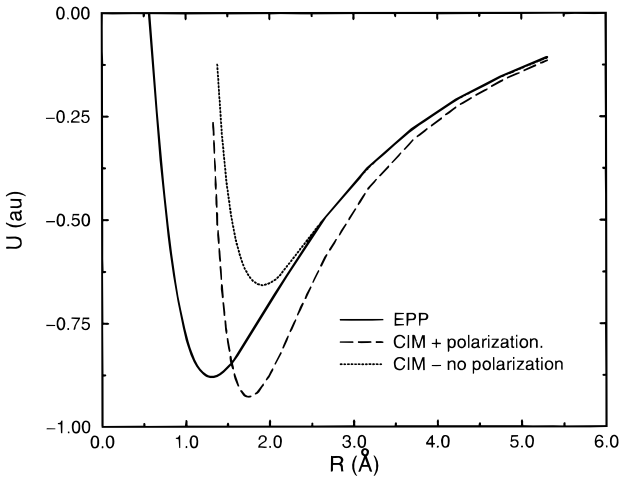

Figure 2. MgO molecular potential energy curves for the EPP and CIM with and without dipole polarization effects. All curves are with respect to $O^- + e^-$.

TABLE 3: Dispersion Parameters Derived from the Polarizabilities in Table 1; See Text for Details

coordination number	C_6^{O-O}/au	C_6^{Mg-O}/au	C_8^{O-O}/au	C_8^{Mg-O}/au
1	309.0223	7.9683	5937.853	112.636
2	198.8372	6.7643	3820.657	90.351
3	132.7426	5.8095	2550.649	73.822
4	94.2830	5.0988	1811.648	62.215
5	71.8829	4.5921	1381.230	54.324
6	57.4147	4.2072	1103.223	48.550

TABLE 4: Ion-Pair Equilibrium Separation, *R*, and Energy for the CIM with No Polarization Effects, CIM with Bulk Polarization, CIM with Full Polarization, and the EPP Derived from the Same Bulk Data; Also Listed Are the Three Watson Sphere Values[16] and the Experimental Value[27]

	R/Å	ΔH_f°/kJ mol^{-1}
"free"	1.75	900
+1	1.67	444
+2	1.56	163
expt	1.75	4 ± 84
CIM	1.91	714
CIM + bulk polarization	1.80	588
CIM + polarization	1.75	0
EPP	1.30	378

III. Calculations

A. Ion Pair. Figure 2 shows the potential energy, *U*, vs bond length, *R*, curves for the MgO molecule for the simple EPP (without polarization effects) and the CIM with and without the dipole polarization effects. The experimental bond length is 1.75 Å.[27] The current equilibrium bond lengths are summarized in Table 4 along with the energies at the minima. The EPP equilibrium bond length is much shorter than that observed experimentally. The "breathing" effect of the CIM leads to an increase in the equilibrium bond length with respect to the simple EPP, toward a value much more in keeping with the experimental value. The addition of dipole polarization effects reduces the equilibrium bond length as would be expected.

Table 4 also lists the equilibrium energies compared with the experimental value and the Watson sphere calculation.[16] Both the basic CIM and EPP give energies outside the (large) experimental range, as does the CIM using the bulk oxide polarizability.

The calculated dipole moment is 5.72 D compared with the experimental value of 6.26 D.[28] If we accept the true transfer-

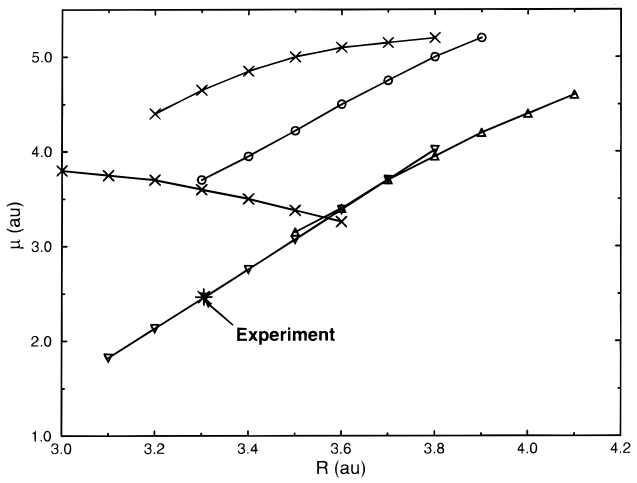

Figure 3. Total dipole moment (μ) against anion−cation separation (R) compared with the SCF *ab initio* data.[18] Key: (×) SCF MgO, (+) SCF CaO, (○) SCF BaO, (△) SCF BaO, (▽) current CIM, (★) experimental equilibrium geometry value.

ability of the short-range CIM parameters, then the required Mg−O bond length, R, and the experimental dipole moment, μ^{expt}, allow a unique $\{\alpha, b^{\text{sr}}\}$ parameter set to be derived. If our model has been constructed in a physically reasonable fashion, then this parameter set should be similar to that derived in section II from more general scaling arguments. This procedure yields $\alpha = 31.35$ au and $b^{\text{sr}} = 1.8343$, which are very similar to the original parameters ($\alpha = 33.651$, $b^{\text{sr}} = 1.80$), demonstrating the general applicability of the model parametrization. The current EPP dipole moment is 12.5 D, while the formal charge dipole moment, for a system with formal charges, no polarization effects, and the experimental bond length, is 16.8 D. The dipole moment is particularly sensitive to subtle changes in the potential model.

The calculated vibrational frequency is 695 cm^{-1}, compared with the experimental value of 785 cm^{-1}.[27]

The CIM gives an equilibrium separation, binding energy, dipole moment, and vibrational frequency in good agreement with experiment. All of these observables are vastly superior to those calculated using the EPP and demonstrate the greater transferability of the CIM representation.

The calculated behavior of the dipole moment with bond length (Figure 3) shows a linear dependence on R like the *ab initio* SrO and BaO curves but unlike MgO. This behavior is a direct consequence of the model. As R increases the "permanent" dipole moment (that due to the ±2 charges) increases linearly ($\mu^{\text{perm}} = 2R$). The anion-induced dipole contribution (which acts to oppose μ^{perm}) is reduced as the electric field on the anion site is reduced (as R^{-2}). However, the overlap contribution (which acts in the same direction as μ^{perm}) is also reduced. The latter two effects effectively cancel on the scale of μ^{perm}, leading to the near linear behavior.

Insight into the "anomalous" behavior of MgO comes from extensive *ab initio* calculations of Fowler and Sadlej.[20] There is an avoided crossing between the ionic ($Mg^{2+}\cdots O^{2-}$) and covalent (Mg···O) states at around the equilibrium separation. The result is that a SCF ground state wave function Mulliken population analysis shows a net charge on the oxygen of $-1.63e$ at $R = 3.0$ au, but only $-0.25e$ at $R = 4.5$ au.[20] Although absolute values calculated in this manner are generally untrustworthy, there is a clear trend in the overall charge. This is fully consistent with the behavior shown in Figure 3. The model, which is based on the ionic description, cannot hope to reproduce this behavior. However, this is not a crucial drawback, as we are only interested in the ion pair in terms of its equilibrium properties, where the ionic model is clearly the most appropriate starting point. Additionally, the larger Madelung potential in the clusters will favor the ionic description.

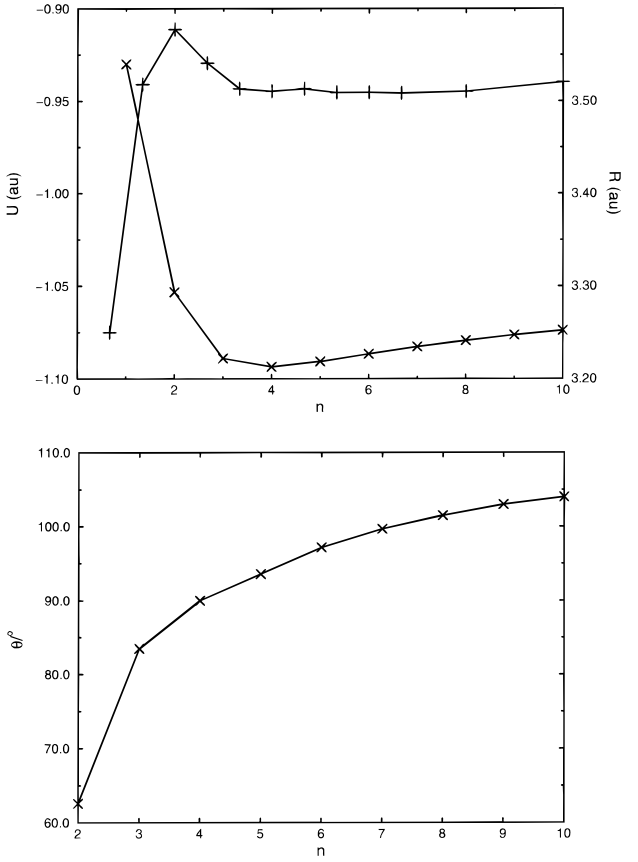

Figure 4. Single rings: (a) energy per molecule vs ring size (×), anion−cation equilibrium separation vs ring size (+), (b) Mg−O−Mg bond angle vs ring size.

B. Clusters. Having established the effectiveness of our parametrization in both the crystalline (ref 14) and ion-pair environments, the next stage is to consider various plausible cluster structures. Our strategy is to consider each "class" of structure (single ring, double rings, cube fragments, etc.) individually.

1. Single Rings. Figure 4a,b shows the energy/cluster size (n) curve for the fully relaxed single rings along with the Mg−O−Mg bond angles. Figure 9a shows some examples of the relaxed structure. Also shown is the nearest-neighbor anion−cation separation, R, vs n. As $n \rightarrow \infty$, $R \rightarrow 3.51$ au, $U \rightarrow -1.07$ au, and $\theta^{\text{Mg-O-Mg}} \rightarrow 105°$ as the rings become so large such that only the nearest-neighbor and next-nearest-neighbor interactions become significant, resulting in the same ring "rumple". Note that the fully relaxed structures have a very different geometry from the unrelaxed, the latter being those identified in the *ab initio* calculations.

2. Double Rings. For the double rings (two rings on top of one another) the energy minimum is at $n = 6$ with $U = -1.103$ au, compared with the single-ring minimum of -1.094 au at $n = 4$. As $n \rightarrow \infty$ $U \rightarrow -1.09$ au. Thus, the double rings are more stable than the single rings of the same size except for the smallest cluster size at $n = 4$. This reflects the stability of the higher coordinate structures. The difference in the inter-/intraring stress is highlighted by the differing R^{intra} and R^{inter} (Figure 5). For $n = 4$ $R^{\text{intra}} = R^{\text{inter}}$ as all the Mg−O units are equivalent, while for $n > 20$ the two separations converge. In between $R^{\text{inter}} < R^{\text{intra}}$, a trend also observed in the HF

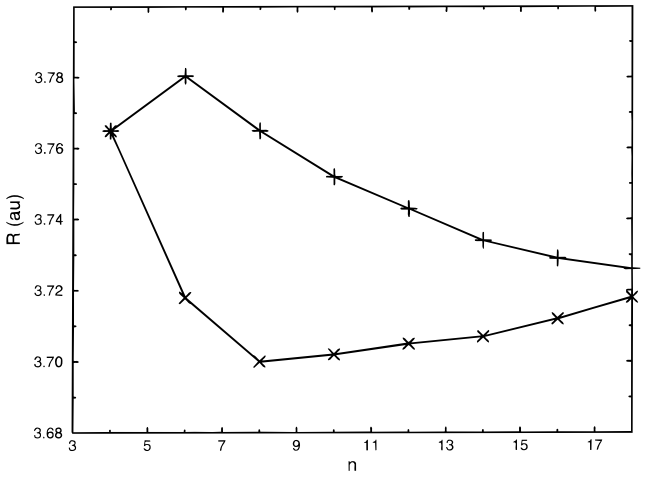

Figure 5. Inter- (×) and intra- (+) ring anion−cation separation for the double rings.

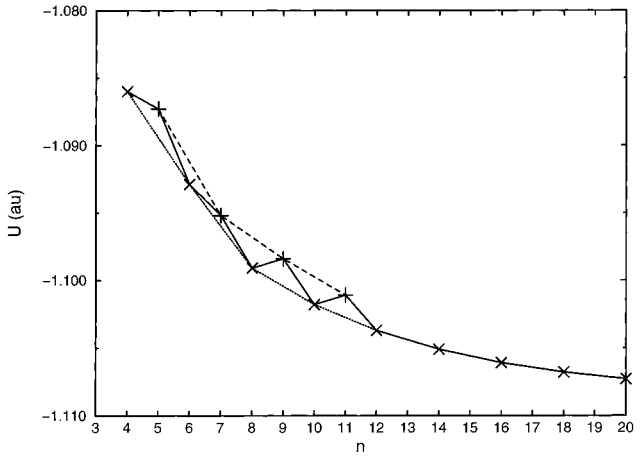

Figure 6. Energy against cluster size (*n*) for the chain cube structures. The lower curve (×, joined by the dotted line) is for even *n*. The upper curve (+, joined by the dashed line) is for the odd *n* fragments having a "molecular flap".

calculations on fixed geometry double rings.[7] This arises because of the significant interactions present beyond the nearest neighbors (in these cases across the ring) which are larger in the smaller rings and act to try to expand the ring.

3. Chain Cubes. Next we consider the chain cube fragments: clusters built up of stacking $n = 2$ rings (nanotubes with two molecules per cross-sectional unit). The clusters with complete cubes (even *n*) are energetically favored over those having an MgO "flap" (odd *n*), as shown in Figure 6. This result is fully consistent with the HF calculations.[7] As $n \rightarrow \infty$, $U \rightarrow -1.11$ au. At $n > 8$ these cubic chains become energetically favored over the double and single rings.

Analogous nanotubes of hexagons and octagons can also be constructed with $U \rightarrow -1.119$ au and -1.118 au, respectively, as $n \rightarrow \infty$. Note that the hexagon-based chains are energetically favored over both the cube- and octahedron-based chains. Some examples of the stable relaxed hexagonal tube structures are shown in Figure 9b.

4. Bulk Fragments. The final step is to consider the "bulk" fragments, that is, sections from the B1 crystal ground state. Figure 7 shows the minimum energies of a selection of cubic fragments in the range $8 \leq n \leq 108$ divided into subgroups based on the number of MgO molecules along each cubic axis. More cubic fragments are energetically favorable over flatter structures of the same size. For example, there are two structures based on $n = 64$ for $1 \times 4 \times 4$ and $2 \times 2 \times 4$ (*x* times *y* times *z* molecules along each axis). The more cubic $2 \times 2 \times 4$ structure is energetically favored over the "flat" $1 \times 4 \times 4$ by ~10 kJ mol^{-1}.

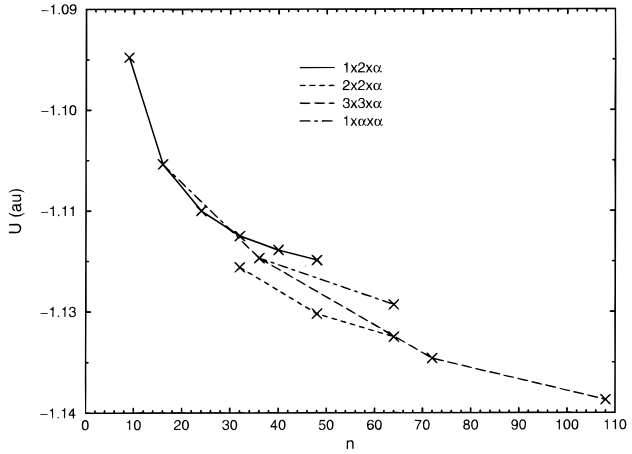

Figure 7. Energy of the bulk structure (B1) fragments against cluster size indicating how the more cubic fragments are favored.

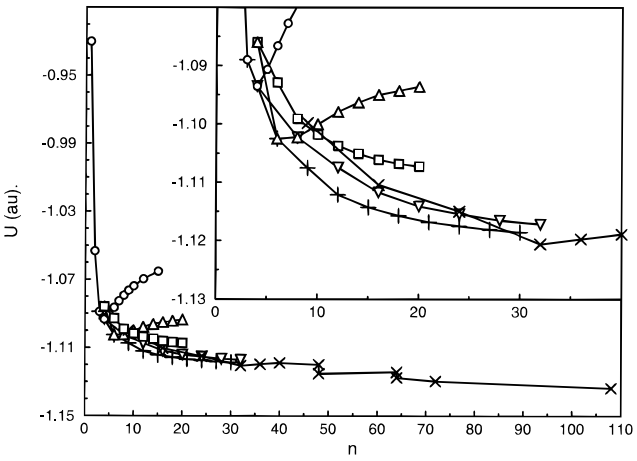

Figure 8. Energy against cluster size for all fragments. The inset shows an expansion to highlight the low cluster size region of stability based on stacking hexagons. Key: □, chain cubes; △, double rings; ○, single rings.

TABLE 5: Fixed and Relaxed Geometry Ring Anion−Cation Separations, *R*, and Energies, *U*, for the CIM and EPP Compared with the Hartree−Fock Values[7]

	HF		CIM				EPP	
			fixed		relaxed			
ring size	*R*	*U*	*R*	*U*	*R*	*U*	*R*	*U*
1	1.739		1.750	−0.930	1.750	−0.930	1.296	−0.881
2	1.836	274.4547	1.944	−0.9693	1.897	−1.0533	1.607	−1.012
3	1.867	274.5042	1.923	−0.9937	1.893	−1.0890	1.589	−1.093
4	1.932	274.5211	1.915	−0.9975	1.874	−1.0935	1.577	−1.117
5	1.936	274.5162	1.912	−0.9977	1.859	−1.0906	1.572	−1.127
6			1.911	−0.9974	1.859	−1.0866	1.570	−1.133

Figure 8 brings together all the energy vs cluster size information. Above $n = 30$ the cubic fragments become favored over the various nanotubes. This is, of course, consistent with the B1 ground state: bulk MgO does *not* consist of extended nanotubes or as a large ring. These cubic fragments are, however, *less* stable than the hexagonal tubes in the range $8 \leq n \leq 30$.

Table 5 compares the bond lengths obtained in the current model with the HF calculations of Recio *et al.*[7] for the *fixed geometry* rings. Also shown are the values obtained with the EPP. These are consistently smaller than the CIM and HF values, the latter two being around the same magnitude. The

TABLE 6: Comparison of the Current Model Anion−Cation Separations for Relaxed Bulk Fragments with DFT Calculations;[8] The Value in Parentheses Is the Mean Bond Length

	R/au		*U*/au	
n	CIM	DFT	CIM	DFT
4	1.99	1.94	−1.0860	−1.087
9	1.940−2.174 (2.031)	1.98	−1.0998	−1.128
16	1.942−2.115 (2.039)	1.99	−1.1104	−1.145
24	1.978−2.163 (2.053)	2.01	−1.1150	−1.157
32	1.992−2.137 (2.058)	2.02	−1.1206	−1.164
bulk	2.103		−1.157	

HF values rise with *n*, while the CIM values jump between $n = 1$ and $n = 2$ and then fall.

A further comparison can be made between our *fully relaxed* CIM structures and the DFT results of Veliah *et al*.[8] Table 6 lists the nearest-neighbor separations and energies for five cubic clusters in the range $n = 4-32$. In the CIM the bond lengths are expressed as a range for the four largest clusters, as there are several inequivalent $Mg^{2+}-O^{2-}$ ion pairs and several bond lengths. For the DFT calculations only one value is quoted, and it is not clear whether this is a mean value. However, both the CIM bond lengths and energies are consistent with the *ab initio* calculations. The original CIM parametrization involved fitting to *ab initio* calculations that reproduce the experimental bulk lattice properties including the energy (=−3038 kJ mol^{-1} [29]). The DFT calculations are clearly tending to a more negative lattice energy.

IV. Discussion

Two results immediately stand out from the cluster calculations. Firstly, as would be expected (and hoped), the clusters based on B1 fragments become favored for the larger cluster sizes ($n \geq 30$). Secondly, clusters based on stacking hexagonal nanotubes are favored in the range $8 \leq n \leq 30$. The mass spectrum shows distinct peaks in the higher mass ranges, consistent with the cubic fragments being most stable.[1] The low−medium mass range shows distinct peaks at $n = 6$, 9, 12, 15, 18, 24, 27, and 30, consistent (with the exception of $n = 21$) with the region in which the current model predicts the hexagonal tubes to be stable over the B1 fragments.

The effect of including polarization effects is to lower the symmetry of the low-energy clusters. In the absence of such effects, for example, the lowest energy $n = 3$ structure is a near perfect hexagon. In the further absence of like−like repulsive terms and dispersion (both of which act to distinguish between the Mg−Mg and O−O pairs) the hexagon is absolutely perfect, the shape being governed entirely by the anion−cation short-range and Coulombic terms. The formation of the hexagon follows the general ionic model principles applicable in the *solid* state. The anion−cation coordination number is maximized with the constraint that the like−like terms are minimized. The inclusion of the polarization effects acts to lower the Mg−O−Mg bond angles by the same mechanism as observed in both the solid and liquid.[10] The dipole induced on the central oxide anion acts to introduce negative charge density between the two Mg's, effectively *screening* their Coulombic interaction. The results are the equilibrium structures in Figure 9a. Polarization also affects the relative energetics of the three-dimensional cluster structures. The types of open clusters favored by formal charge EPPs *without* polarization (see, for example, Figure 5 in ref 1) are favored, as the requirement to minimize the like−like Coulombic repulsion is a large driving force. The polarization effects lead to more acute Mg−O−Mg bond angles and hence favor more closely packed structures: the increase in like−like repulsion is more than counterbalanced by the polarization energy.

In the B1 crystal fragments the polarization effects act in the same manner, although they are much less significant for the nonsurface ions. In Figure 9c, for example, polarization effects act to narrow the Mg−O−Mg angles for oxides at corners. Such effects are also clear in the DFT results (Figure 1 of ref 8).

The factors governing cluster stability are as follows. In purely ionic model terms each ion wishes to attain its full first-coordination sphere, favoring the formation of bulklike fragments. Polarization effects favor more asymmetric anion environments by wishing to maximize the dipole stabilization energy. In particular the asymmetry requirement favors both a reduction in anion coordination number and the formation of

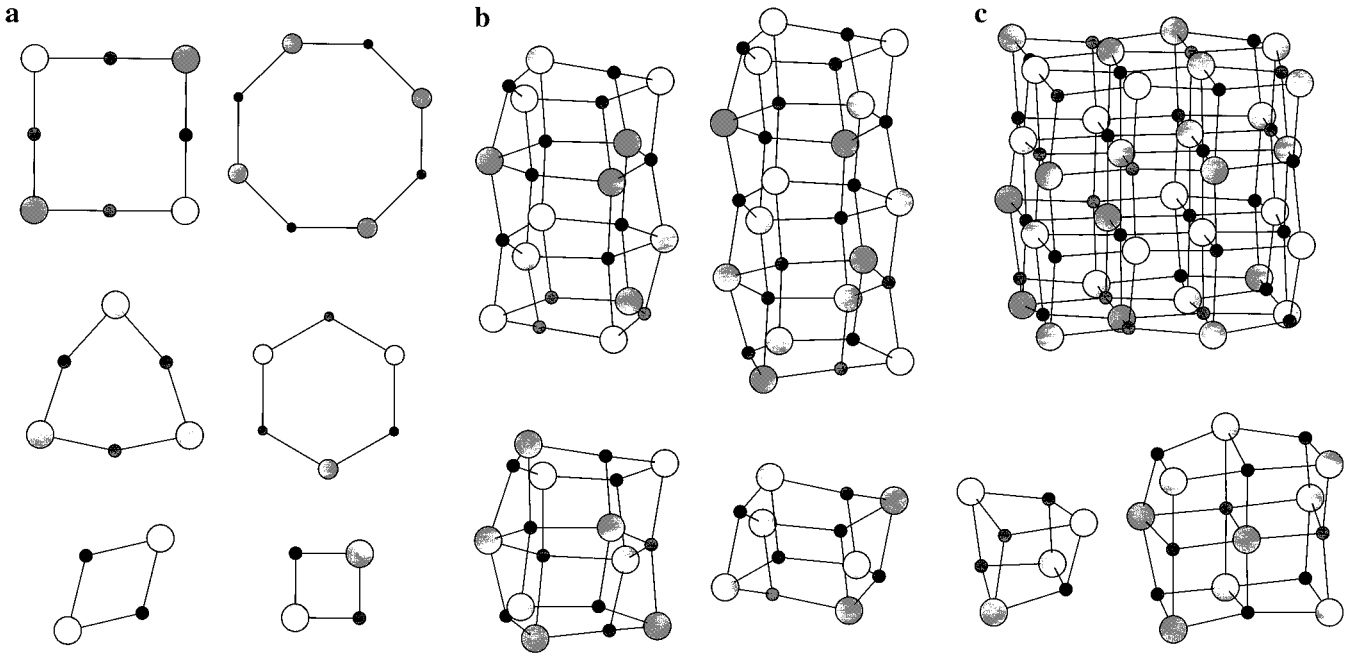

Figure 9. Example relaxed cluster geometries: (a) single rings ($n = 1$, 2, 3) relaxed (left) and unrelaxed; (b) four example relaxed stacked hexagon structures; shown are the 6, 9, 12, and 15 molecule configurations; (c) three relaxed bulk fragments ($n = 4$, 9, 32).

surface sites. In the condensed environments, for example, dipole polarization effects are most significant when the anions have low coordination (i.e. in SiO_2[10]). In terms of the structure of small clusters this second requirement maximizing *surface* sites is critical. The hexagon-based nanotubes represent the ideal balance between the ionic driving forces and the polarization effects in the small−medium size cluster range *for this specific system*: the number of anion surface sites are maximized, allowing for the largest possible induction stabilization energies. As the cluster size increases, the driving force for an ion to attain its full first coordination shell becomes dominant over polarization energies available at undercoordinated sites.

The Ziemann/Castleman EPP based on unit charges gives more closed (close-packed) structures[1] reminiscent of the CIM with full polarizability. A general observation is that the lowering of formal charges in some way mimics polarization effects (for example, a charge of 0.74*e* for the ion pair would reproduce the experimental dipole moment without the need for polarization). The use of partial charges is not desirable, as the objective is to produce models that are truly *transferable* over as wide a range of state points as possible. The use of variable charges does not generally lend itself to flexible modeling. Additionally, the variation of the ion charge must necessarily alter the physical meaning of the other model parameters, again in a nontrivial way. In the case of the charge reduction the systems are simply becoming Lennard-Jonesian while the inclusion of polarization effects screened the like−like charge interactions largely responsible for the open structures. As a result, both mechanisms lead to closer packed structures. Furthermore, Ziemann and Castleman state that fitting the old shell model to the monomer is "difficult". This is the result of the overlying restrictive mechanical representation of the underlying physics afforded by the shell model, which is inherently not well-suited to parametrization for environments as far removed from the solid state as the ion pair. The current work clearly shows anion polarization effects to be vital in producing understandable cluster geometries. This finding is in apparent contradiction to that of Ziemann and Castleman, who conclude that the description of polarization afforded by the shell model provides little or no advantage over the EPP. In fact, we would agree with this finding but argue that the inclusion of polarization effects is crucial, but *it is the shell model that is inappropriate* because of its inherent inflexibility.

As for the ion pair, both the compressible-ion and polarization effects are crucial in obtaining "reasonable" geometries. For the fixed ring geometries in Table 5 the use of the EPP is, as predicted from the ion-pair discussion, clearly inappropriate. The nearest-neighbor anion−cation separations are far too short: The oxide anion is effectively not repulsive enough. The inclusion of polarization effects on top of the EPP would, of course, magnify this shortcoming.

The stability of the hexagon-based $(MgO)_n$ nanotubes in the low-mass range clearly identifies this system with LiF rather than NaCl or KCl. The latter two systems favor bulklike fragments over virtually the whole of the mass range. Our above argument is that it is the polarization effects that act to favor the hexagon-based units over the bulk fragments. This may well hold true for the three alkali halides, although it is impossible to tell without further potential model calculations. Although the F^- ion is much less polarizable than Cl^- (typically 6−8 au compared with 19−24 au), the Li^+ cation is much smaller than either the Na^+ or K^+. Thus, the smaller polarizability is offset by the larger electric fields at the anion sites, which are the direct result of the smaller anion−cation separations. The indications are that there is a very fine balance in the model between the bulk and nonbulk fragments, with the latter favored by increased polarization effects.

V. Conclusions

In this paper it has been shown how a compressible-ion model extended to include the effect of coordination-dependent anion polarizability can describe small cluster properties for MgO. For $n > 32$ clusters based on fragments of the B1 ground state are found to dominate, consistent with the mass spectrum. In the lower mass range units based on $(MgO)_3$ stacked hexagons (nanotubes) are found to be energetically favorable over the cubic options. This is again consistent with the experimental mass spectra, which show distinct peaks at intervals of $n = 3$. In this sense, therefore, the $(MgO)_n$ clusters can be identified with those calculated for LiF rather than those for NaCl or KCl.

The compressible-ion model itself has been previously shown to give excellent intercrystalline transferability and can give the same excellent level of transferability to the "ultimate extreme", the ion pair, as long as the dependence of the anion dipole polarization on coordination number is accounted for. As with the previous work in this area, the strategy is to parametrize each term from independent sources rather than fitting an assumed energy function to total energy calculations. The variable-polarizability aspect of the model is, in this spirit, derived from Hartree−Fock calculations that focus on this property both in the bulk and in a series of undercoordinated sites. The dispersion terms are linked directly to these polarizabilities in a standard manner.

The above discussion has important implications for the future direction of *ab initio* calculations. These calculations are necessarily computationally expensive, and so the energy minimizations have been generally applied to fixed geometries for each proposed cluster. However, the CIM calculations clearly show that alternative structures are likely to have a lower energy than those studied. For example, the ring-based clusters are less symmetric due to anion polarization. The way forward, therefore, is to treat the potential models and *ab initio* calculations as *complementary*. The potential model, having been shown to give a good representation of the ion pair and crystal extrema, can give important clues as to structures worthy of the *ab initio* treatment.

Such *ab initio* calculations will allow for a more flexible description of the anion polarizability in which it depends on coordination number in a smooth manner. This will allow the dynamical nature of the model to be fully exploited.

Acknowledgment. The author would like to thank Professor Paul Madden for many useful discussions and for many helpful suggestions regarding the final manuscript. The author would also like to thank the Royal Society for financial support.

References and Notes

(1) Ziemann, P. J.; Castleman, A. W., Jr. *J. Chem. Phys.* **1991**, *94*, 718.
(2) Saunders, W. A. *Phys. Rev. B* **1988**, *37*, 6583.
(3) Saunders, W. A. *Z. Phys. D.* **1989**, *12*, 601.
(4) Sedlmayer, E. *Interstellar Dust. Proc. IAU Symp. No. 135*; Allamandola, L. J., Tielens, A. G. G. M., Eds.; D. Reidel Publ. Co.: Dordrecht, p 467.
(5) Ochsenfeld, C.; Ahlrichs, R. *Ber. Bunsen.-Ges. Phys. Chem.* **1994**, *98*, 34.
(6) Ahlrichs, R.; Ochsenfeld, C. *Ber. Bunsen-Ges. Phys. Chem.* **1992**, *96*, 1287.
(7) Recio, J. M.; Pandey, R.; Ayuela, A.; Kunz, A. B. *J. Chem. Phys.* **1993**, *98*, 4783.
(8) Veliah, S.; Randey, R.; Li, Y. S.; Newsam, J. M.; Vessal, B. *Chem. Phys. Lett.* **1995**, *235*, 53.
(9) Henrich, V. E. *Rep. Prog. Phys.* **1985**, *48*, 1481.

(10) Madden, P. A.; Wilson, M. *Chem. Soc. Rev.* **1996**, *25*, 399.
(11) Pyper, N. C. *Proc. R. Soc. London* **1995**, *A352*, 89.
(12) Fowler, P. W.; Madden, P. A. *J. Phys. Chem.* **1985**, *89*, 2581.
(13) Fowler, P. W.; Madden, P. A. *Mol. Phys.* **1983**, *49*, 913.
(14) Wilson, M.; Madden, P. A.; Pyper, N. C.; Harding, J. H. *J. Chem. Phys.* **1996**, *104*, 8068.
(15) Wilson, M.; Schönberger, U.; Finnis, M. W. *Phys. Rev. B* **1996**, *54*, 9147.
(16) Tossell, J. A. *Am. Mineral.* **1980**, *65*, 163.
(17) Fowler, P. W.; Tole, P. *Surf. Sci.* **1988**, *197*, 457.
(18) Pacchioni, G.; Illas, F. *Chem. Phys.* **1995**, *199*, 155.
(19) Wilson, M.; Cabral, B. J. C.; Madden, P. A. *J. Phys. Chem.* **1996**, *100*, 1227.
(20) Fowler, P. W.; Sadlej, A. J. *Mol. Phys.* **1991**, *73*, 43.
(21) Wilson, M.; Madden, P. A. *J. Phys.: Condens. Matter* **1994**, *6*, 159.
(22) Sangster, M. J. L.; Dixon, M. *Adv. Phys.* **1976**, *23*, 247−342.
(23) Slater, J. C.; Kirkwood, J. G. *Phys. Rev.* **1931**, *37*, 682.
(24) Starkschall, G.; Gordon, R. G. *J. Chem. Phys.* **1972**, *56*, 2801.
(25) Jacobi, N.; Csanak, G. *Chem. Phys. Lett.* **1975**, *30*, 367.
(26) Tang, K. T.; Toennies, J. P. *J. Chem. Phys.* **1984**, *80*, 3726.
(27) Huber, K. P.; Herzberg, G. *Molecular Spectra and Molecular Structure IV. Constants of Diatomic Molecules*; Van Nostrand Reinhold: New Jersey, 1979.
(28) Büsener, H.; Heinrich, F.; Hese, A. *Chem. Phys.* **1987**, *112*, 139.
(29) Cohen, A. J.; Gordon, R. G. *Phys. Rev. B* **1979**, *14*, 4593.